Available online at www.sciencedirect.com
SCIENCE DIRECT®
Journal of the European Ceramic Society 25 (2005) 749–757
www.elsevier.com/locate/jeurceramsoc

Fracture behavior of poled piezoelectric PZT under mechanical and electrical loads

H. Jelitto [a,*], H. Keßler [b], G. A. Schneider [a], H. Balke [b]

[a] *Technische Universität Hamburg-Harburg, Advanced Ceramics Group, Denickestr. 15, D-21073 Hamburg, Germany*
[b] *Technische Universität Dresden, Institut für Festkörpermechanik, D-01062 Dresden, Germany*

Received 16 October 2003; received in revised form 20 February 2004; accepted 25 February 2004

Available online 7 June 2004

Abstract

Four point bending samples were poled parallel to the long axis, notched and fractured. During mechanical loading, a constant electric field was applied parallel or antiparallel to the poling direction (perpendicular to the crack surface). Assuming electrical crack boundary conditions of (i) an impermeable or (ii) a completely permeable crack, the stress intensity factors K_I and the field intensity factors K_{IV} at failure were determined by linear-piezoelectric finite element calculations. The fracture curve $K_{IC}(K_{IV})$ for the impermeable crack model does not comply to fracture criteria based on the total energy release rate or on the mechanical energy release rate. Within the completely permeable crack model, it appears generally impossible to describe electric field effects on the fracture resistance. Some theoretical extensions of the crack models are discussed which might contribute to resolve the aforementioned problems.
© 2004 Elsevier Ltd. All rights reserved.

Keywords: Fracture; Piezoelectric properties; Ferroelectric materials; Toughness and toughening; PZT

1. Introduction

Piezoelectric PZT ceramics are important materials employed in the fabrication of electromechanical devices like actuators, sensors, and transducers. In this context, the fracture behavior of poled PZT under combined electromechanical load conditions is an important issue, as PZT is susceptible to brittle fracture.[1]

There are partially contradictory statements in the literature regarding the effect of an applied electric field on the fracture resistance of PZT materials poled perpendicular to the crack:

(i) Park and Sun[2] and Tobin and Pak[3] report that positive electric fields (parallel to the poling direction) promote and negative electric fields (opposite to the poling direction) impede crack propagation. These conclusions are based on three point bending and compact tension experiments,[2] and on indentation fracture tests at relatively low indentation loads of about 5 N.
(ii) At higher indentation loads of about 20 N, Park and Sun found that an electric field independent of its orientation facilitates crack propagation.[2] The same trend was confirmed by Fu and Zhang[4] in compact tension and indentation fracture experiments with an indentation load of about 50 N and by Schneider and Heyer[5] at indentation loads of 40 N.
(iii) Finally, Wang and Singh[6] observed in indentation fracture tests with an indentation load of about 12 N that positive electric fields inhibit and negative electric fields enhance crack propagation.

In our experiment, we use a four point bending device to investigate PZT ceramic bars poled in longitudinal direction (normal to the prospective crack surface). The fracture tests are conducted at constant electric field (E_a) applied parallel or antiparallel to the poling direction, where E_a is defined by the applied voltage (V) divided by the distance between the electrodes (l). In the remaining part of this introduction, we present some preliminary considerations regarding the presentation of fracture data by phenomenological curves and regarding the electrical crack boundary conditions.

1.1. Phenomenological fracture curves

Raw data as load and applied electric field measured at failure in a fracture experiment are influenced by specimen

* Corresponding author.
E-mail address: h.jelitto@tu-harburg.de (H. Jelitto).

0955-2219/$ – see front matter © 2004 Elsevier Ltd. All rights reserved.
doi:10.1016/j.jeurceramsoc.2004.02.022

geometry and crack length. Therefore, the intrinsic, geometry independent fracture resistance of the material cannot be described directly in terms of these data.

In modeling our experiment, we adapt the standard fracture mechanics approach of K-dominated fracture in the presence of a small process zone at the crack tip[7,8] to our situation of electromechanical (K_I–K_{IV}) mixed mode fracture: For all measured failure loads and the corresponding applied electric fields, the mode I stress intensity factor (K_I) and the electric displacement intensity factor (K_{IV}) are determined by linear-piezoelectric finite element calculations. K_I and K_{IV} characterize the strength of the square root singularities at the crack tip of the stress and electric displacement components perpendicular to the crack, respectively.[9] The fracture resistance of the PZT-material is tentatively characterized by the phenomenological curve of the stress intensity factor at failure as a function of the electric displacement intensity factor, $K_I = K_{IC}(K_{IV})$.

This model relies on the existence of a so-called K-dominated region near the crack tip with linear material behavior and singular stress/strain and electric field/electric displacement distributions which, with a sufficient degree of accuracy, depend only on the intensity factors K_I and K_{IV} of the linear-piezoelectric field problem corresponding to the applied external boundary conditions. An eventual nonlinear process zone should be embedded well within the linear K-dominated region. In piezoelectrics, the source of nonlinearity in the process zone is presumably domain switching. Under such small scale conditions, the state of the material in the process zone depends solely on the intensity factors K_I and K_{IV} of the surrounding K-dominated region. Therefore, the function $K_{IC}(K_{IV})$ should characterize the intrinsic fracture resistance if only failure of the material is initiated in the process zone or in the surrounding K-dominated region. This concept was already applied to the same PZT material fractured by conducting cracks.[10]

1.2. Impermeable and completely permeable electrical crack boundary conditions

A complication stems from the electrical boundary condition on the nonconducting crack surfaces which is not well defined. Crack problems of this type can be classified according to their normalized crack opening, defined as the ratio of crack opening to crack length times the ratio of the permittivity of the solid to the permittivity of the medium in the crack.[12] Widely open cracks in that sense are approximately impermeable for the electric displacement flux and have a maximum discontinuity of the electric potential between the crack faces.[9,12] Cracks with small opening displacements are approximately permeable and have a continuous electric potential.[11–13] Both types of crack boundary conditions lead to linear-piezoelectric field problems. The model of a partially permeable crack extrapolates between the two limiting cases of a completely permeable and an impermeable crack,[14–16] and is closer to reality as shown experimentally by Schneider et al.[17] However, the semipermeable crack boundary conditions are nonlinear and more difficult to handle. For this reason, we analyze our fracture data, using only the permeable and the impermeable crack model. As a drawback, we can at best provide bounds for the fracture resistance, even if the assumption of a small scale switching zone is correct.

The following properties of the stress intensity factor (K_I) and of the electric displacement intensity factor (K_{IV}) of impermeable and completely permeable cracks are validated (for our configuration) by the results of the finite element calculations in Appendix A: for given load conditions, specimen geometry and crack length, K_I of an impermeable crack is equal to K_I of the corresponding permeable crack. For both types of crack boundary conditions, K_I depends only on the mechanical load (F), not on the applied electric field (E_a), $K_I = K_I(F)$. K_{IV} of an impermeable crack is a function of F and E_a, $K_{IV} = K_{IV}(F, E_a)$. K_{IV} of a completely permeable crack is proportional to K_I, $K_{IV} = \text{constant} \times K_I(F) \equiv K_{IV}(F)$ where the proportionality constant depends only on the material properties and on the orientation of the crack relative to the poling direction of the material. The latter statement is a general property of permeable cracks. Therefore, measuring fracture curves $K_I = K_{IC}(K_{IV})$, we can expect $K_I = K_{IC}(K_{IV}(F, E_a))$ for impermeable cracks and $K_I = K_{IC}(K_{IV}(F))$ for completely permeable cracks. In other words, from the impermeable and the permeable crack models, only the impermeable model can be fitted to fracture data which depend on the applied electric field. The permeable crack model predicts that fracture should not be influenced by an electric field at all, leading to a constant fracture toughness K_{IC}—a reconfirmation of McMeekings statement.[16]

2. Experimental set up

Commercial morphotropic PZT ceramic bars (PIC 151, PI-Ceramic GmbH, Lederhose, Germany) of dimensions 3 mm × 4 mm × 24 mm were fractured in a standardized four-point-bending device equipped with a 1 kN-load cell (type S2, HBM GmbH, Darmstadt, Germany), using ASTM-compliant[18] support distances of 10 and 20 mm. The principal set up is shown in Fig. 1.

The samples were prepared as follows: After a heat treatment at 500 °C for 2 h, the specimens were poled in the longitudinal direction between their small end surfaces; these were electroded by silver paint coatings. Upon poling, five specimens were connected parallel at a time and placed in Fluorinert-liquid (FCM 77, 3 M, dielectric strength 17 kV/mm) in order to inhibit flashovers. The applied voltage of 35 kV, corresponding to an electric field of 1.46 kV/mm, was above the coercive field of about 0.8 kV/mm and yielded homogeneously poled specimens. Later during the fracture experiments, the silver paint

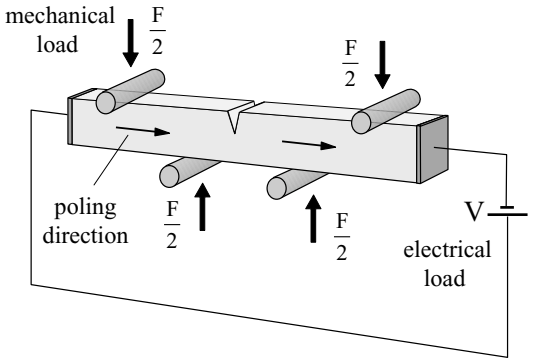

Fig. 1. Principal arrangement of the specimen and loads.

electrodes were used to generate a lower electric field applied parallel or antiparallel to the poling direction. The notch was cut with a diamond saw blade of 120 μm thickness and sharpened with a razor blade in a special mechanical appliance (SEVNB).[19,20] Using diamond paste of 6, 2.5, and 1 μm grain size, the curvature radius of the notch tip was reduced to less than 10 μm. The notch depths of the 31 specimen comprised three groups of $a \approx 1.1$, 1.5, 2.0 mm corresponding to relative notch depths of $\alpha \approx 0.28$, 0.37, 0.5 when normalized by the sample widths (w).

During the fracture experiments, the maximum voltage of $V = 18$ kV, corresponding to $E_a = 0.75$ kV/mm field strength, required a slight modification of the bending device. For the purpose of insulation, the four loading cylinders made of hardened steal were replaced by four ceramic Al_2O_3-cylinders. The cylinders had to be fixed and aligned by rubber bands instead of the four original magnetic plates; these were replaced by glass plates of approximately the same size (see Fig. 2). Nevertheless, it was necessary to perform the experiment in Fluorinert-liquid completely covering the specimen.

A mechanical loading rate of about 3 N/s was applied by a computer controlled universal testing machine (ATS Series 1600, Applied Test Systems, Butler, USA) at a feed rate of 0.2 μm/s. Sometimes during the first measurements, the upper loading cylinders moved slightly or twisted a few tenth of a millimeter to the side upon specimen contact. An inspection of their cross sections revealed a diameter variation of about 20–50 μm along their perimeter. After grinding the ceramic cylinders with a 'center less grinding machine' (Fa. A. Schweizer GmbH, Forchheim, Germany) to an accuracy of better than 5 μm, the motion and twist upon specimen contact disappeared. The remaining scatter in the experimental data was less than 5%.

3. Results and discussion

Fig. 3 shows the loads at fracture (F_c) measured at different applied electric fields (E_a). These fracture data are still geometry dependent: At fixed electric field, the fracture load decreases with crack length (a). Therefore, the function $F_c(E_a, a)$ by itself cannot characterize the fracture resistance of the material.

3.1. Phenomenological fracture curve

Depending on the adopted crack boundary conditions—completely permeable or impermeable crack—each set of fracture loads and crack lengths was converted into stress intensity and electric displacement intensity factors, $K_{IC} = K_I(F_c, a)$ and $K_{IV}(F_c, E_a, a)$. F_c, the mechanical load measured at fracture, depends on the applied electric field and

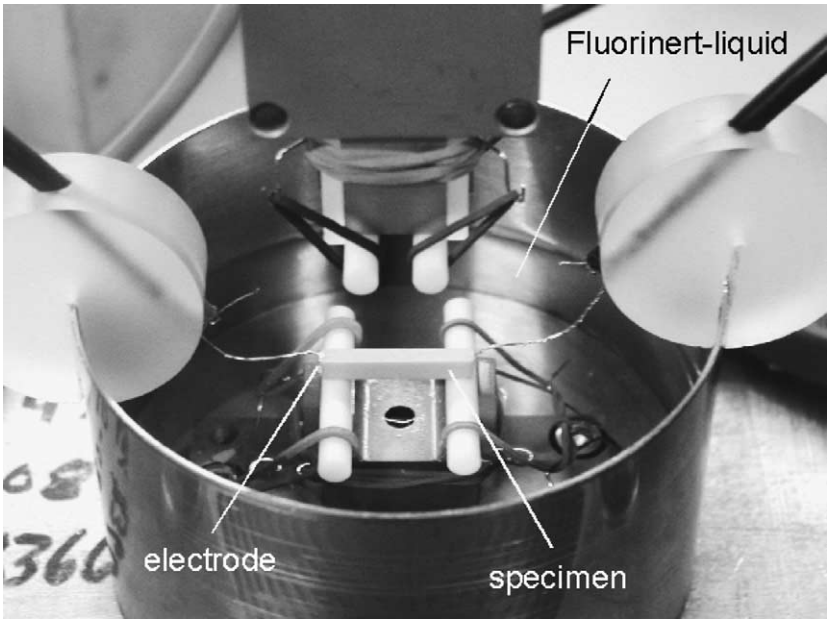

Fig. 2. Experimental set up. (In contrast to the measurement, the Fluorinert-liquid is not covering the specimen on the photograph.)

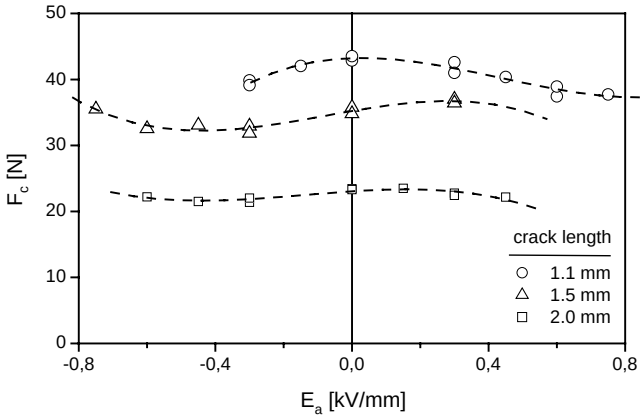

Fig. 3. Measured fracture loads (F_c) as a function of the applied electric field (E_a).

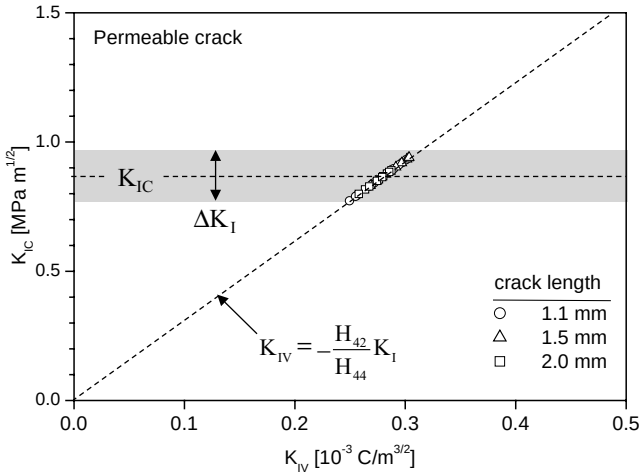

Fig. 4. Intensity factors at fracture for the permeable crack model.

on the crack length, $F_c = F_c(E_a, a)$, as shown in Fig. 3. The functions $K_I(F, a)$ and $K_{IV}(F, E_a, a)$ were determined by the finite element method as described in Appendix A. Figs. 4 and 5 show the calculated intensity factors at fracture.

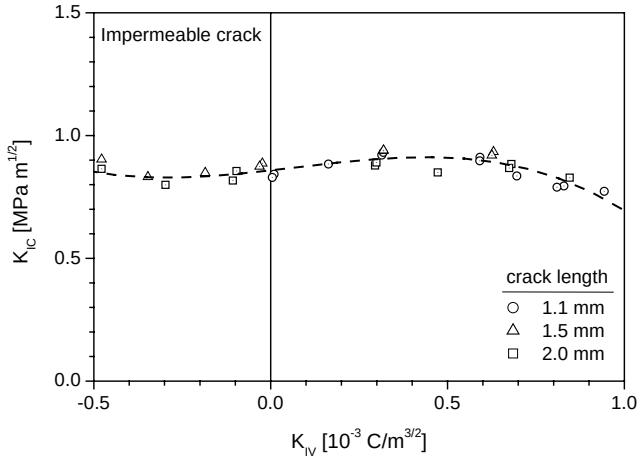

Fig. 5. Intensity factors at fracture for the impermeable crack model.

Fig. 4 corresponds to permeable crack boundary conditions. Due to the proportionality of K_I and K_{IV} for permeable cracks, the data points form a straight line. The variation ΔK_I of about 20% makes it impossible to consider the fracture toughness as a strictly constant value. Thus, the permeable crack model should be discarded at this moment for the reasons discussed at the end of the introduction.

Fig. 5 shows the K_I–K_{IV} fracture data, if the crack is considered electrically impermeable. The data points can be fitted by the cubic polynomial

$$K_{IC}(K_{IV}) = 0.9\,\mathrm{MPa}\sqrt{m}\left[1 + 0.2\left(\frac{K_{IV}}{10^{-3}\mathrm{C/m^{3/2}}}\right) + 0.1\left(\frac{K_{IV}}{10^{-3}\mathrm{C/m^{3/2}}}\right)^2 - 0.5\left(\frac{K_{IV}}{10^{-3}\mathrm{C/m^{3/2}}}\right)^3\right] \quad (1)$$

Eq. (1) represents the phenomenological fracture resistance curve resulting directly from the measured fracture loads and the additional ad hoc assumption of impermeable crack boundary conditions. In order to move beyond a purely phenomenological curve, we should look for possible physically based fracture criteria.

3.2. Energy criteria of fracture

Energy criteria predict initiation of fracture when the local energy release rate at the crack tip (G) becomes equal to a material specific energy barrier (G_c)

$$G = G_c \quad (2)$$

Eq. (2) represents the balance of supplied and dissipated energy during fracture. If large scale effects such as crack bridging are not present, the energy release rate can be given completely by crack closure integrals calculated for a virtual crack advance (ΔA)[9]

$$G = \lim_{\Delta A\to 0}\int_{\Delta A}\frac{\boldsymbol{t}\Delta\boldsymbol{u}}{2}\,\mathrm{d}A + \lim_{\Delta A\to 0}\int_{\Delta A}\frac{(\boldsymbol{n}^+\cdot\boldsymbol{D})\Delta\varphi}{2}\,\mathrm{d}A = G_m + G_e \quad (3)$$

where the superscripts, $(\cdot)^+$ and $(\cdot)^-$, denote the two opposite crack faces. $\boldsymbol{t}$ is the traction vector on the prospective crack surface before and $\Delta\boldsymbol{u} = \boldsymbol{u}^+ - \boldsymbol{u}^-$ the crack opening displacement vector between the opposite crack faces after the virtual crack advance. Similarly, $\boldsymbol{n}^+\cdot\boldsymbol{D}$ represents the normal electric displacement vector on the prospective crack surface before and $\Delta\varphi = \varphi^+ - \varphi^-$ the electric potential jump between the opposite crack faces after the virtual crack advance. For obvious reasons, G_m and G_e are called the mechanical and electrical energy release rate, respectively, although it is generally impossible to split the total energy into purely mechanical and electrical parts in materials with piezoelectric coupling.[16] Independently of the applied load conditions—fixed force or fixed displacement,

fixed voltage or fixed charge—the crack closure integrals can be expressed by the field intensity factors,[9]

$$G_{\mathrm{m}} = \frac{1}{4}\sum_{i=1}^{3}\sum_{k=1}^{4} H_{ik} K_i K_k \quad \text{and} \quad G_{\mathrm{e}} = \frac{1}{4}\sum_{k=1}^{4} H_{4k} K_4 K_k \quad (4)$$

resulting in the total energy release rate

$$G = \tfrac{1}{4}\boldsymbol{K}\cdot\boldsymbol{H}\cdot\boldsymbol{K}^T \quad (5)$$

where the electric displacement intensity factor K_{IV} is combined with the stress intensity factors K_{I}, K_{II}, K_{III}.

$$\boldsymbol{K} = (K_{\mathrm{II}}, K_{\mathrm{I}}, K_{\mathrm{III}}, K_{\mathrm{IV}}) \quad (6)$$

and the symmetric Irwin matrix ($\boldsymbol{H}$) depends on the material properties and on the orientation of the crack with respect to the material. Only K_{I} and K_{IV} are different from zero in a four point bending experiment. Using the Stroh formalism,[9] the corresponding elements of the Irwin matrix for PZT PIC 151 were calculated as[21]

$$\begin{pmatrix} H_{22} & H_{24} \\ H_{42} & H_{44} \end{pmatrix} = \begin{pmatrix} 45.1\times10^{-12}\,\mathrm{m^2/N} & 39.7\times10^{-3}\,\mathrm{m^2/As} \\ 39.7\times10^{-3}\,\mathrm{m^2/As} & -123\times10^{6}\,\mathrm{V^2/N} \end{pmatrix} \quad (7)$$

The electrical energy release rate (G_{e}) of impermeable cracks is always negative[9] due to $H_{44} < 0$ and Eq. (4). In permeable cracks, G_{e} is always zero due to the continuous electric potential on the crack, $\Delta\varphi = 0$, and Eq. (3). Noting the equivalence of $\Delta\varphi = 0$ with[9]

$$H_{24}K_{\mathrm{I}} + H_{44}K_{\mathrm{IV}} = 0 \quad (8)$$

the energy release rate of permeable cracks can be written as

$$G = G_{\mathrm{m}} = \frac{\bar{H}_{22}K_{\mathrm{I}}^2}{4} \quad \text{with} \quad \bar{H}_{22} = H_{22} - \frac{H_{24}^2}{H_{44}} > 0 \quad (9)$$

Thus, the total energy release rate (G) of permeable cracks, depending only on the mechanical loads, is always positive. In the case of impermeable cracks, G depends on both mechanical and electrical loads, but may become negative if the electric field is large.

A straightforward attempt to extend linear-elastic fracture mechanics to electromechanical mixed mode (K_{I}–K_{IV}) loading would invoke an energy criterion with the total energy release rate of impermeable cracks

$$\begin{aligned} G(K_{\mathrm{I}}, K_{\mathrm{IV}}) &= G_{\mathrm{m}}(K_{\mathrm{I}}, K_{\mathrm{IV}}) + G_{\mathrm{e}}(K_{\mathrm{I}}, K_{\mathrm{IV}}) \\ &= \tfrac{1}{4}(H_{22}K_{\mathrm{I}}^2 + 2H_{24}K_{\mathrm{I}}K_{\mathrm{IV}} + H_{44}K_{\mathrm{IV}}^2) = G_{\mathrm{c}} \end{aligned} \quad (10)$$

where G_{c} represents the material specific constant energy barrier. From Eq. (10) one would expect electric field effects on the fracture toughness of dielectric materials even in the case of vanishing piezoelectricity ($H_{24} = 0$). The dashed line in Fig. 6 corresponds to the total energy release rate criterion for an impermeable crack. The critical energy release rate $G_{\mathrm{c}} = 8.3\,\mathrm{J/m^2}$ was calculated from Eqs. (1) and (10) with $K_{\mathrm{IV}} = 0$. The solid line represents the measured fracture curve for our PZT material, Eq. (1). A comparison shows no agreement between the predicted and the measured curve (Eqs. (1) and (10)).

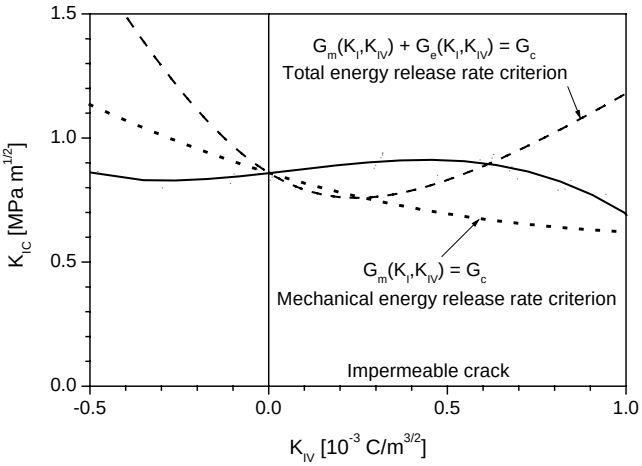

Fig. 6. Comparison of the measured fracture curve (solid, fitted by Eq. (1)) with predictions based on a total energy release rate criterion (dashed) and on a mechanical energy release rate criterion (dotted) for impermeable cracks.

Park and Sun[2] suggested a fracture criterion based on the mechanical energy release rate (G_{m}) of impermeable cracks instead of the total energy release rate (G)

$$G_{\mathrm{m}}(K_{\mathrm{I}}, K_{\mathrm{IV}}) = \tfrac{1}{4}(H_{22}K_{\mathrm{I}}^2 + H_{24}K_{\mathrm{I}}K_{\mathrm{IV}}) = G_{\mathrm{c}} \quad (11)$$

From Eq. (11) one would expect no electric field effects on the fracture toughness of dielectric materials without piezoelectric coupling, $H_{24} = 0$. Fig. 6 compares the prediction (dotted line) and the measured curve (solid line) for our piezoelectric PZT material. Again, there is no agreement. The measurements show a moderately increasing fracture toughness (K_{IC}) with increasing K_{IV} in the surroundings of $K_{\mathrm{IV}} = 0$, and a possibly reversed trend at larger magnitudes of $|K_{\mathrm{IV}}|$, whereas the overall prediction of the mechanical energy release rate criterion suggests a monotonously decreasing K_{IC} with increasing K_{IV}.

3.3. Discussion

Consider the values of the total energy release rate (G) and of the mechanical energy release rate (G_{m}) at fracture as a function of K_{IV} for the impermeable crack (Fig. 7). Obviously, the fracture criterion (10), which is based on the total energy release rate (G), has to be discarded immediately, as G becomes negative in a range of K_{IV}-values where the sample has been fractured. But also a fracture criterion based on the mechanical energy release rate (G_{m}) is questionable as G_{m} cannot be considered to be a constant (G_{c}) as required by (11), even in an approximate sense. This

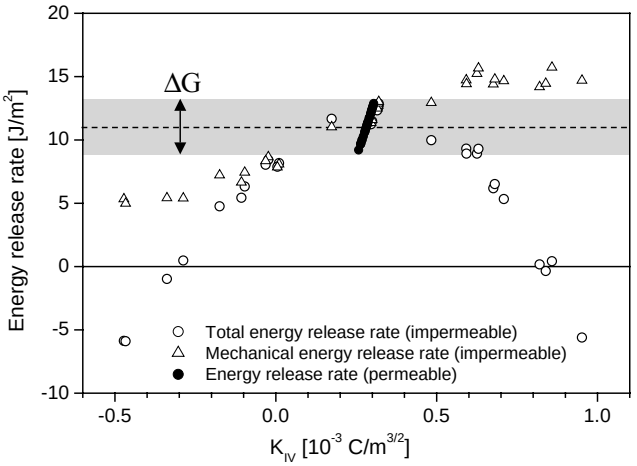

Fig. 7. Energy release rates calculated from the measured intensity factors at failure. The dashed horizontal line indicates the approximate toughness level resulting from a permeable crack assumption.

emphasizes again, that our measurements do not comply with fracture criteria based on the total or mechanical energy release rate of impermeable cracks.

Compare now the very large variations of G or G_m for the impermeable crack model with the range of ΔG for the completely permeable crack (Fig. 7). In view of this comparison, the permeable crack model in conjunction with a simple fracture criterion $G = G_c \approx 12\,J/m^2$ is to be prefered, in spite of the ratio $\Delta G/G_c \approx 30\%$. This is in agreement with recommendations based on a theoretical analysis of partially permeable Griffith cracks by Balke et al.[15] Eq. (9) shows the equivalence of the fracture criteria $G = G_c \approx 12\,J/m^2$ and $K_I = K_{IC} \approx 0.9\,MPa\,m^{1/2}$, similar to linear-elastic fracture mechanics. The critical energy release rate of $12\,J/m^2$ was also measured in four point bending tests of the same PZT material but with conducting cracks.[10]

Within the completely permeable crack model, we have to accept the impossibility to account for electric field effects on the fracture toughness. Real cracks, however, are electrically semipermeable, not completely impermeable or completely permeable.[14–16] Thus, Kelvin force microscopy measurements of the dielectric constant inside the crack of $\varepsilon_r = 40$ support a partial permeability of the crack for electric fields,[17] inspite of the fact that cracks in the experiment are never mathematically sharp, representing instead long notches with noncontacting faces that are separated by an insulating medium. The semipermeable crack model leaves hope to improve the analysis of our fracture data for a better account of electric field effects. The boundary value problems to be solved in this case are nonlinear due to the semipermeable boundary conditions on the crack faces. Besides the usual contributions from the crack closure integrals, the energy release rate gains additional contributions from the electric field inside the crack. In a simple picture, these contributions should be determined by the volume of the open crack times a characteristic energy density of the electric field, thus being proportional to the crack opening displacement $\sim K_I$ times the square of the electric field $\sim K_{IV}^2$ leading to $G \sim K_I K_{IV}^2$—compare with an analytical treatment of the semipermeable Griffith crack under constant farfield load.[22] Strictly speaking, terms $\sim K_I K_{IV}^2$ are also present in permeable cracks. However, due to the required small crack opening condition for permeable cracks, they can be usually neglected. For other than Griffith cracks, the energy release rate of semipermeable cracks has to be calculated in each particular geometry and load configuration. Similar to large scale bridging effects or other effects related to a large process zone, the contributions of the electric field inside the crack to the energy release rate cannot be expressed in a standardized manner by the intensity factors.[16]

Besides the permeability of the crack, Landis indicated an electrically induced traction between opposite crack surfaces and remanent polarization surface charges as additional physical features of piezoelectric crack problems, which might be important for the fracture analysis but are usually neglected. In addition, polarization switching near the crack tip could influence by crack shielding or amplification the measured fracture toughness,[23,24] and it is important to model these effects in combination with the correct crack surface conditions.

If the applied electric field and therefore the switching zone at the crack tip become too large, the small scale switching assumption behind the K-concept ceases to be valid. The size of the switching zone (R_s) can be estimated similar to the plastic zone size for small scale yielding in Irwin's approach:[8] The yield stress and the fracture toughness of Irwin's approach have to be replaced by $\varepsilon_{33}E_c$ and $K_{IV,C}$, respectively. Assuming a permeable crack with $K_{IC} \approx 0.9\,MPa\,m^{1/2}$ and $K_{IV,C} = -K_{IC}H_{24}/H_{44}$, using the Irwin matrix elements of Eq. (7), the permittivity $\varepsilon_{33} = 850\varepsilon_0$ and a coercive field of $E_c = 0.8\,kV/mm$, the size of the switching zone is determined as

$$R_s \approx \frac{1}{2\pi}\left(\frac{K_{IV,C}}{\varepsilon_{33}E_c}\right)^2 = \frac{1}{2\pi}\left(\frac{H_{24}K_{IC}}{H_{44}\varepsilon_{33}E_c}\right)^2 \approx 0.3\,mm \quad (12)$$

A process zone of $R_s = 0.3\,mm$ at the tip of 1–2 mm long cracks could be already large enough to be critical for the small scale switching assumption.

4. Summary and conclusions

Our fracture data and analysis do not comply with fracture criteria based on the total or mechanical energy release rate of impermeable cracks. They are better reproduced by a constant fracture toughness criterion, $G(K_I) = G_c$, based on a permeable crack model and supported by Kelvin force microscopy measurements.[17] The toughness values determined for insulating and conducting cracks in our PZT material are $G_c \approx 12\,J/m^2$.

The reasons for the disagreement between our experimental results on the one hand and statements in the literature

regarding electric field effects on the fracture toughness and their interpretation based on the mechanical energy release rate of impermeable cracks[2] on the other hand are not clear.

The permeable crack model adopted in our analysis makes it impossible to account for electric field effects on the fracture toughness and has a rather large variation of the energy release rate $\Delta G/G_c$. This implies that a semipermeable crack model should be used in an improved analysis. Furthermore, direct and independent measurements of the energy release rate by a generalized piezoelectric compliance method would be desirable.[25,26] They could eliminate the influence of the particular assumptions used for the crack boundary conditions on the calculated energy release rates.

In view of a relatively large estimated crack tip process zone, the small scale switching assumption used in the analysis needs further substantiation.

Acknowledgements

We would like to thank Professor R.M. McMeeking (University of California, Santa Barbara) and Professor T.-Y. Zhang (Hongkong University of Science & Technology) for useful and stimulating discussions.

Appendix A. Finite element model

The four-point-bending configuration was modeled by four-noded piezoelectric plane strain elements using the finite element code ANSYS. The electric field (E_a) was applied between the electroded side faces of the specimen (perpendicular to the crack) parallel or antiparallel to the poling direction. The simulation results can be applied to different edge crack lengths, applied loads and electric fields. However, any change in the specimen geometry or material properties would require a new simulation.

Specimen geometry and material properties

The specimen beyond the outer load points does not exert a significant influence on the crack tip conditions. For this reason, the finite element model with the dimensions listed in Table A.1 was restricted to the region of length s_0 between the outer load points. The transversally isotropic material constants of PZT PIC 151 are listed in Table A.2.

Table A.1
Specimen geometry

Width, w (mm)	≈4
Thickness, t (mm)	≈3
Length, l (mm)	24
Outer span, s_o (mm)	20
Inner span, s_i (mm)	10

Table A.2
Material constants for PZT PIC 151

Stiffness constants	Piezoelectric constants	Permittivity constants
$C_{11} = 107.65\,\text{GPa}$	$e_{31} = -9.6\,\text{C/m}^2$	$\varepsilon_{11} = 1110\varepsilon_0$
$C_{12} = 63.124\,\text{GPa}$	$e_{33} = 15.1\,\text{C/m}^2$	$\varepsilon_{33} = 852\varepsilon_0$
$C_{13} = 63.854\,\text{GPa}$	$e_{15} = 12.0\,\text{C/m}^2$	
$C_{33} = 100.45\,\text{GPa}$		
$C_{44} = 19.624\,\text{GPa}$		

Edge crack geometry and boundary conditions

The crack length (c) normalized by the specimen width (w) was varied between $\alpha = 0.05$ and $\alpha = 0.95$ in steps of 0.05. The crack faces are traction free.

Two types of electric crack face conditions were applied to the insulating crack:

1. The impermeable crack with vanishing normal electric displacement components.
2. The completely permeable crack with continuous electric potential and normal electric displacements.

Employing the geometric and material symmetry, the permeable crack conditions are enforced by fixing the electric potential on crack faces and ligament to one half of the applied voltage.

Intensity factors

The intensity factors as a function of crack length, applied load and applied electric field were calculated as follows:

1. A finite element model was built for each normalized crack length between $\alpha = 0.05$ and $\alpha = 0.95$.
2. For each crack length, two load cases were simulated:
   (a) a prescribed four point bending load and zero applied electric field
   (b) a prescribed applied electric field and zero bending load

   Mixed loading can be represented as linear superposition of the load cases (a) and (b).
3. For each load case, stresses and electric displacements were evaluated at five test nodes in the ligament. The distance of these nodes to the crack tip were chosen as $0.1c$, $0.15c$, $0.2c$, $0.25c$, and $0.3c$, where c is the smaller length of crack length and ligament length.
4. The singular electromechanical fields were extrapolated to the crack tip as

$$\sqrt{2\pi x} \cdot \sigma_y = K_I + A_I x \tag{A.1}$$

$$\sqrt{2\pi x} \cdot D_y = K_{IV} + A_D x \tag{A.2}$$

where the x- and y-directions of the crack tip coordinate system are parallel and perpendicular to the crack surface, respectively. The parameters K and A are least-square fits to the numerically calculated data at the five test nodes in the ligament. The linear fit is based on the absence

of T-stresses and electric displacements for the analyzed field components (C.F. Gao, private communication). The load dependence of the calculated intensity factors can be represented as:

$$K_{\mathrm{I}} = w^{1/2}\sigma_a k_{\mathrm{I}\sigma}(\alpha) + w^{1/2}E_{\mathrm{a}}e_{33}k_{\mathrm{IE}}(\alpha) \quad (A.3)$$

$$K_{\mathrm{IV}} = w^{1/2}\sigma_a \frac{e_{33}}{C_{33}}k_{D\sigma}(\alpha) + w^{1/2}E_{\mathrm{a}}\varepsilon_{33}k_{\mathrm{DE}}(\alpha) \quad (A.4)$$

where $\sigma_a = (3/2)(F/t)(s_{\mathrm{o}} - s_{\mathrm{i}})/w^2$ gives the applied bending stress of an uncracked sample loaded by the same bending force (F). D_y and the intensity factors K_{IV} are counted positive in the poling direction. The shape functions of the normalized crack length (α), $k_{\mathrm{I}\sigma}(\alpha)$, …, $k_{\mathrm{DE}}(\alpha)$, can be approximated by least-square fits and are listed below. A relative error can be estimated as the absolute value of the difference between fit curve and actual k-value normalized by the k-value. In all cases, the average error was less than 1%, the maximum error for all data points somewhat more than 3%. $k_{\mathrm{I}\sigma}(\alpha)$ for the impermeable and permeable crack are equal and close to $k_{\mathrm{I}\sigma}(\alpha)$ for a conducting crack which was analyzed for comparison.

Shape functions for impermeable cracks

$$k_{\mathrm{I}\sigma} = \frac{\sqrt{\pi\alpha}}{(1-\alpha)^{3/2}}(1.07 - 1.89\alpha + 2.14\alpha^2 - 0.95\alpha^3) \quad \text{and}$$
$$k_{\mathrm{IE}} = 0 \quad (A.5)$$

$$k_{D\sigma} = \frac{\sqrt{\pi\alpha}}{(1-\alpha)^{3/2}}(2.45 - 4.33\alpha + 4.73\alpha^2 - 2.06\alpha^3) \quad (A.6)$$

$$k_{\mathrm{DE}} = \sqrt{\frac{\pi\alpha}{1-\alpha}}(2.05 - 1.19\alpha + 0.48\alpha^2 - 0.61\alpha^3) \quad (A.7)$$

Shape functions for completely permeable cracks

$$k_{\mathrm{I}\sigma} = \frac{\sqrt{\pi\alpha}}{(1-\alpha)^{3/2}}(1.07 - 1.89\alpha + 2.14\alpha^2 - 0.95\alpha^3) \quad \text{and}$$
$$k_{\mathrm{IE}} = 0 \quad (A.8)$$

$$k_{D\sigma} = \frac{\sqrt{\pi\alpha}}{(1-\alpha)^{3/2}}(2.33 - 4.12\alpha + 4.59\alpha^2 - 2.02\alpha^3) \quad \text{and}$$
$$k_{\mathrm{DE}} = 0 \quad (A.9)$$

The shape functions, Eqs. (A.5)–(A.9), take into account the asymptotes of the intensity factors for $\alpha \to 0$ and $\alpha \to 1$, similar to the functional form of standard reference solutions in edge cracked beam problems.[27]

For permeable cracks, Eqs. (A.3), (A.4), (A.8), and (A.9) show that the field intensity factor K_{IV} is proportional to K_{I}. Within a numerical error of <2%, the calculations confirm the generally valid crack length independent proportionality relation between K_{I} and K_{IV} for permeable cracks

$$K_{\mathrm{IV}} = -\frac{H_{42}}{H_{44}}K_{\mathrm{I}} \quad (A.10)$$

The Irwin matrix elements H_{42} and H_{44} depend only on the material constants and on the orientation of the crack with respect to the material.[9] For PZT PIC 151, they are given by Eq. (7).

References

1. Freiman, S. W. and Pohanka, R. C., Review of mechanically related failures of ceramic capacitors. *J. Am. Ceram. Soc.* 1989, **72**(12), 2258–2263.
2. Park, S. and Sun, C.-T., Fracture criteria for piezoelectric ceramics. *J. Am. Ceram. Soc.* 1995, **78**(6), 1475–1480.
3. Tobin, A. G. and Pak, Y. E., Effect of electric fields on fracture behavior of PZT ceramics. *Proc. SPIE Int. Soc. Opt. Eng.* 1993, **1916**, 78–86.
4. Fu, R. and Zhang, T. Y., Effects of an electric field on the fracture toughness of poled lead zirkonate titanate ceramics. *J. Am. Ceram. Soc.* 2000, **83**(5), 1215–1218.
5. Schneider, G. A. and Heyer, V., Influence of the electric field on Vickers indentation crack growth in $BaTiO_3$. *J. Eur. Ceram. Soc.* 1999, **19**, 1299–1306.
6. Wang, H. and Singh, R. N., Crack propagation in piezoelectric ceramics: effects of applied electric fields. *J. Appl. Phys.* 1997, **81**(11), 7471–7479.
7. Lawn, B., *Fracture of Brittle Solids* (*2nd ed.*). Cambridge Solid State Science Series, Cambridge University Press, 1993.
8. Anderson, T. L., *Fracture Mechanics, Fundamentals and Applications* (*2nd ed.*). CRC Press, London, 1995.
9. Suo, Z., Kuo, C.-M., Barnett, D. M. and Willis, J. R., Fracture mechanics for piezoelectric ceramics. *J. Mech. Phys. Solids* 1992, **40**(4), 739–765.
10. Heyer, V., Schneider, G. A., Balke, H., Drescher, J. and Bahr, H.-A., A fracture criterion for conducting cracks in homogeneously poled piezoelectric PZT-PIC 151 ceramics. *Acta Mater.* 1998, **46**(18), 6615–6622.
11. Parton, V. Z., Fracture mechanics of piezoelectric materials. *Acta Astronautica* 1976, **3**, 671–683.
12. McMeeking, R. M., Electrostrictive stresses near crack-like flaws. *J. Appl. Math. Phys.* 1989, **40**, 615–627.
13. Zhang, T.-Y. and Hack, J. E., Mode-III cracks in piezoelectric materials. *J. Appl. Phys.* 1992, **71**(12), 5865–5870.
14. Hao, H. and Shen, Z. Y., A new electric boundary condition of electric fracture mechanics and its applications. *Eng. Fract. Mech.* 1992, **47**(6), 793–802.
15. Balke, H., Kemmer, G. and Drescher, J., Some remarks on fracture mechanics of piezoelectric solids. In *Proc. Micro Mat '97*, ed. B. Michel and T. Winkler. Berlin, 1997, pp. 398–401.
16. McMeeking, R. M., Crack tip energy release rate for a piezoelectric compact tension specimen. *Eng. Fract. Mech.* 1999, **64**, 217–244.
17. Schneider, G. A., Felten, F. and McMeeking, R. M., The electrical potential difference across cracks in PZT measured by Kelvin Probe Microscopy and the implications for fracture. *Acta Mater.* 2003, **51**, 2235–2241.
18. *ASTM C1161-90*. American Society for Testing and Materials, Philadelphia, PA.
19. Kübler, J., *Bestimmung der Bruchzähigkeit keramischer Werkstoffe mit der SEVNB Methode: Resultate eines VAMAS/ ESIS Ringversuches*. EMPA, Werkstoffwoche, 1998.
20. Kübler, J., Fracture toughness of ceramics using the SEVNB method: from a preliminary study to a standard test method. In *Fracture Resistance Testing of Monolithic and Composite Brittle Materials, ASTM STP 1409*, ed. J. A. Salem, M. G. Jenkins and G. D. Quinn.

American Society for Testing and Materials, West Conshohocken, PA, 2001.
21. Kemmer, G., *Berechnung von elektromechanischen Intensitätsparametern bei Rissen in Piezokeramiken, Fortschritt-Berichte VDI, Reihe 18, Nr. 261*. VDI Verlag, Düsseldorf, 2000 [in German].
22. Zhang, T. Y., Zhao, M. H. and Tong, P., Fracture of piezoelectric ceramics. *Adv. Appl. Mech.* 2002, **38**, 147–289.
23. Yang, W. and Zhu, T., Switch-toughening of ferroelectrics subjected to electric fields. *J. Mech. Phys. Solids* 1998, **46**(2), 291–311.
24. Zeng, X. and Rajapakse, R. K. N. D., Domain switching induced fracture toughness variation in ferroelectrics. *Smart Mater. Struct.* 2001, **10**, 203–211.
25. Suo, Z., Mechanics concepts for failure in ferroelectric ceramics, Smart structures and materials. In *ASME, AD-Vol 24/AMD-Vol 123*. 1991, pp. 1–6.
26. Guiu, F., Algueró, M. and Reece, M. J., *Philos. Mag.* 2003, **83**(7), 873–888.
27. Murakami, Y., *Stress Intensity Factors Handbook*, Pergamon Press, Oxford, New York, 1987.